Ultrafast Electron Microscopy

DOI: 10.1002/ange.201205093

Environmental Scanning Ultrafast Electron Microscopy: Structural Dynamics of Solvation at Interfaces**

*Ding-Shyue Yang, Omar F. Mohammed, and Ahmed H. Zewail**

Interfacial forces, in particular the ones involving solvation dynamics and chemical reactivity, are critical to a range of phenomena, including those of heterogeneous catalysis and corrosion.[1,2] Various surface-sensitive techniques have been developed, and, for most studies, imaging is made under the conditions of a high or ultrahigh vacuum and/or without sufficient time resolution. The development of environmental electron microscopy[3–7] has relaxed the first constraint, and time-resolved spectroscopic methods[8–13] have extended the temporal resolution to the femtosecond domain. As a consequence of the diffraction limit of light, however, these all-optical measurements acquire an ensemble-averaged signal over a region of tens of micrometers of the specimen. To overcome this limit and probe structural dynamics locally, a technique with simultaneous space and time resolutions is needed. These atomic-scale resolutions can be achieved using four-dimensional ultrafast electron microscopy (4D UEM)[14,15] in the transmission mode, but for interfaces one must utilize a probe that is capable of scanning but only sensitive to the surface atoms or molecules.

Our method of choice is scanning ultrafast electron microscopy (S-UEM).[16,17] In this scanning mode, we use two ultrashort pulses, one for initiating the change in a fixed region and another to generate an electron probe for scanning. The impingement of the imaging, primary electron (PE) pulse leads to the emission of secondary electrons (SEs), which originate from the nanometer-thick surface region, because of their low energy and small escape depth.[18] Therefore, the observed signals result from accumulation of the secondary electrons generated by individual impinging primary electrons under the influence of a change caused by the surface dynamics. In the present study, the secondary electrons experience a difference in the work function at the surface and consequently the probability of their escape is altered, thus providing the change for mapping surface dynamics. For transmission imaging, a cell must enclose the specimen and confine the ambient gas (or liquid) to maintain the high vacuum required for the operation of a transmission electron microscope.[4] In the case of environmental scanning electron microscopy,[6,7,19] the emitted SEs from the specimen acquire additional kinetic energy on their way to a positively biased detector and ionize the gas molecules or atoms encountered in the chamber through inelastic collisions. A cascade amplification of SEs results and can be collected (Figure 1). The positive ions may drift toward the specimen and compensate for surface charges, a useful feature when imaging insulating materials.[7] The approach enables the imaging of various surfaces, whether conducting or insulating, dry or wet, and at different PE energies.[6,7,19,20]

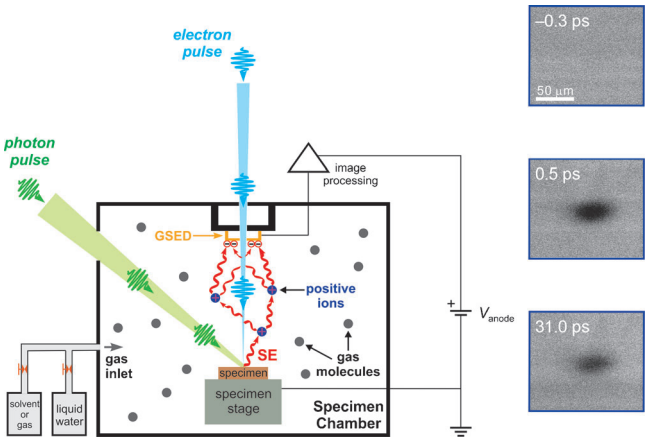

Figure 1. Environmental S-UEM (schematic) and three experimental frames at −0.3, 5.0, and 31.0 ps. Shown are the two pulses involved, the primary electron probe and the clocking optical pulse that initiates the change. The delay between the two pulses determines the time steps that can be made (1 μm optical path corresponds to 3.3 fs), and the time resolution is determined by the pulse width of both, as reported in Ref. [17]. Construction of images at a given delay time is achieved through the scanning process on the specimen surface; the image frames shown here are for the CdSe($10\bar{1}0$) surface in polar ambient conditions. GSED = gaseous secondary electron detector.

Here, we introduce environmental S-UEM as a method for real-space imaging of interfacial dynamics and reactivity under various ambient conditions as well as heterogeneity. Crystalline CdSe interfaces, whose potential applications are of considerable interest,[21] were employed as prototype systems. When photons of the clocking light pulse impinge on the specimen surface, energetic carriers are generated through the above-gap excitation. The difference in the surface dynamics for polar and nonpolar solvation is evident

[*] Dr. D.-S. Yang, Dr. O. F. Mohammed, Prof. Dr. A. H. Zewail
Physical Biology Center for Ultrafast Science & Technology
Arthur Amos Noyes Laboratory of Chemical Physics
California Institute of Technology
Pasadena, CA 91125 (USA)
E-mail: zewail@caltech.edu

[**] This work was supported by the Air Force Office of Scientific Research and the National Science Foundation in the Gordon and Betty Moore Center for physical biology at Caltech. We thank Prof. Dr. Samir K. Pal for insightful discussions during the initial phase of this work. O.F.M. is grateful for a distinguished scholar award provided by the Arab Fund for Economic and Social Development.

Supporting information for this article is available on the WWW under http://dx.doi.org/10.1002/anie.201205093.

in the images, and the results reveal the essential role of the collective electrostatic reorganization between the dipoles of the adsorbed molecules and the surface.

The structures of the two types of CdSe surfaces studied are shown in Figure 2a; the (0001) surface is terminated by Cd atoms, and the $(10\bar{1}0)$ [and also the $(11\bar{2}0)$] surface contains equal numbers of Cd and Se atoms. The interaction with adsorbate molecules is expected to greatly reduce the surface reconstruction for the latter case.[22–24]

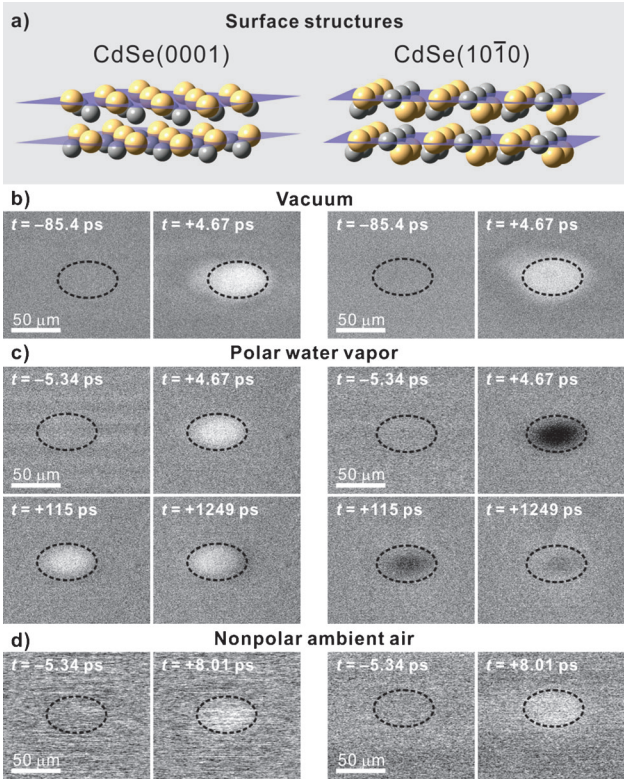

Figure 2. Structures of CdSe surfaces and their environmental S-UEM dynamics. a) Unreconstructed surface structures of CdSe(0001) and (10$\bar{1}$0), with Cd atoms in yellow and Se atoms in gray. b–d) Difference images, referenced to a negative-time frame, of CdSe(0001) (left) and CdSe(10$\bar{1}$0) (right) at the indicated delay times in a high vacuum (b), the surfaces exposed to water vapor (c), and the surfaces exposed to nonpolar ambient air (d). The dashed ellipses indicate the laser-irradiated region at $1/e^2$ of the maximum fluence. At the indicated negative times, the absence of a discernible intensity difference signifies the return of the interfacial structure to the equilibrated state between two consecutive pulses at the repetition rate used. Special attention should be given to the dynamics of CdSe(10$\bar{1}$0) in water vapor (panel c, right), which shows a remarkable opposite change in the contrast at positive times.

Shown in Figure 2b–d are the difference images, that is, the image at time t referenced to an image at negative time, which show the surface dynamics for the following examples of polarity: vacuum, polar solvation with water, and nonpolar ambient air. No change in the contrast was observed before the arrival of the light pulse (i.e., at negative times), thus indicating the recovery of the specimen back to its equilibrated state at the repetition rate used (i.e., 79.3 ns between consecutive excitation events). In a high vacuum, a similar bright contrast was seen immediately after excitation of the surface and only in the laser-irradiated region for both types of surfaces (Figure 2b). We note that at our surface excitation fluence of 55 $\mu J\,cm^{-2}$ (in the absence of the probe electron pulse), no photoemitted electrons were detected by the +500 V biased detector placed directly above the specimen. The trapping of transient photoelectrons near the surface should also be negligible under this electric field.

A similar bright contrast was recorded at positive times for both types of CdSe surfaces in ambient air (Figure 2d) and also for CdSe(0001) exposed to water vapor (Figure 2c, left). In contrast, a distinct darkness was observed in the laser-illuminated region when the CdSe$(10\bar{1}0)$ surface was exposed to water vapor (Figure 2c, right). Given that these observations were made under the same experimental conditions, the results in Figure 2 provide evidence for the major role played by interfacial interactions at the (0001) and $(10\bar{1}0)$ surfaces. Repeating these experiments with other polar adsorbates, including ammonia (1.42 D), methanol (1.69 D), acetone (2.88 D), and acetonitrile (3.96 D), led to the same behavior being observed, namely bright contrast on (0001) and dark contrast on the $(10\bar{1}0)$ surface of CdSe. However, a bright contrast was observed for nonpolar ambient gases, such as oxygen and carbon dioxide, on both surfaces.

Figure 3 displays the intensity (contrast) difference at the center of the laser-irradiated region as a function of time for different surface structures and selected solvents. As shown in Figure 3a, the CdSe(0001) surface exposed to water vapor exhibits positive-time dynamics, whereas the CdSe$(10\bar{1}0)$ surface gives the "opposite" behavior, namely, instead of an increase in signal, we observe an initial decrease and then a recovery. Besides this opposite behavior, we found a time delay of approximately 2 ps for the onset of dynamics on the $(10\bar{1}0)$ surface; a plateau is reached at about 4 ps (Figure 3b). Figure 3b also displays the observed behavior for acetonitrile, which is similar to that of water. The temporal behavior at short and long times is depicted in Figure 3c, and indicates that the recovery takes place on the nanosecond time scale. To confirm the robustness of the behavior we also examined the $(11\bar{2}0)$ surface (Figure 3d).

It should be noted that the observed behaviors in Figure 3 are not the result of an integration over the laser-illuminated area. With real-space imaging, we are able to examine the temporal behavior of a local region (i.e. pixel areas). In this way, the above-mentioned delay recorded for the $(10\bar{1}0)$ surface was found to be reproducible for any local section of the photoexcited region, as evident from the difference images obtained without normalization. Moreover, the dynamics observed for flat surfaces was found to be homogeneous (see Figure 2b–d), which is consistent with the data in Figure 3 being representative of the whole region. Finally, at the present magnification (and therefore field of view), imaging provides an opportunity to probe the influence of fluence on different local areas as a result of the intensity profile of the laser footprint on the specimen; indeed the reported features of the dynamics in Figure 3 are robust over the fluence range covered.

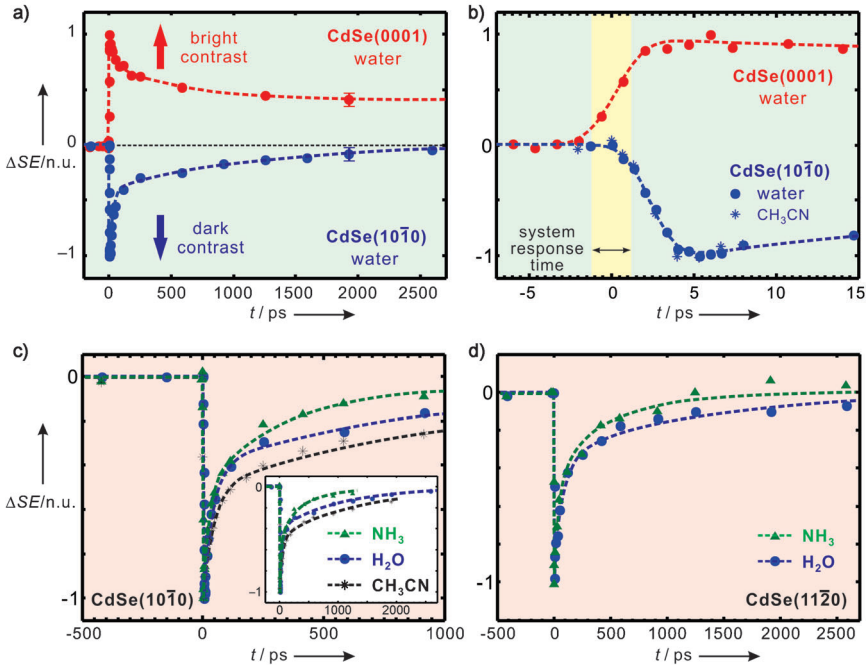

Figure 3. Solvation dynamics of CdSe(0001) and $(10\bar{1}0)$ surfaces. a) Contrast difference at the center of the laser-illuminated region (in the normalized unit) as a function of time, for surfaces exposed to water vapor. The error bars (standard deviation) give the typical level of intensity fluctuation in one SE image. All dashed lines are a guide to the eye. b) Early time dynamics, showing the 2 ps delay in the onset of change for CdSe$(10\bar{1}0)$ in water and acetonitrile vapors. c, d) Long-time dynamics of CdSe$(10\bar{1}0)$ (c) and CdSe$(11\bar{2}0)$ (d) surfaces in the presence of NH_3, H_2O, and CH_3CN.

The temporal and structural behavior in a vacuum (Figure 2b) is understood by considering the enhancement of the SEs, which results in a bright contrast in the temporal changes of images, because of the increased number of electrons promoted from the valence to the conduction band of CdSe.[17] In a vacuum, this is true for both surfaces. Under environmental polar solvation (Figure 2c), the opposite behavior for the (0001) and $(10\bar{1}0)$ surfaces must, therefore, be due to the nature of the surface dipole and the strength of interaction with the adsorbate. As a binary polar material, CdSe has a permanent crystal dipole moment along the *c*-axis. Given the arrangement of surface atoms and the known crystal dipole moment, solvent molecules in the adsorbate layers[25–27] bind in different equilibrium geometries and form their preferential structures on different surfaces (Figure 4, left panels). Upon excitation of the surface, the local surface equilibrium changes, because of the creation of energetic charge carriers, and the structure of the adsorbate layers evolves to the new equilibrium structure (Figure 4, lower right panels; see below). This is reminiscent of the dynamics of molecular solvation in bulk solvents, although a difference is expected for the spatial distribution of solvent molecules around a photoexcited species. Here, we did not resolve the initial inertia dynamics observed in solution-phase studies of water and acetonitrile, and consequently the similar response (Figure 3b) at early times.

According to density functional theory calculations, the preferred orientation of polar adsorbate molecules on CdSe(0001) is along the normal direction of the surface,[23] which is the direction of the prominent crystal dipole moment (see Figure 4b, upper right). In contrast, on CdSe$(10\bar{1}0)$ and $(11\bar{2}0)$ surfaces, the preferred orientation of polar adsorbates is along a tilted direction, with their partial negative charges interacting with the electron-deficit Cd atoms[22–24] (Figure 4a, upper right). The binding energy in both cases ranges from 0.4 to 0.7 eV, with no distinct difference.[23]

The observed dynamics of a 2 ps delay when the CdSe$(10\bar{1}0)$ or $(11\bar{2}0)$ surface is solvated—and the absence of a delay for the (0001) surface—reflects this change of molecule–surface interaction at the interface. When the charge carriers are generated (by the photons) near the CdSe$(10\bar{1}0)$ and $(11\bar{2}0)$ surfaces, the potential of the electrons and holes determines the interaction with adsorbate molecules, through an electrostatic force, thereby causing a collective molecular reorientation and movement only within the laser-illuminated region. The 2 ps delay suggests that the solvent reorientation time for the CdSe$(10\bar{1}0)$ and $(11\bar{2}0)$ surfaces is significantly slower than that of the (0001) surface, and the picosecond time scale is consistent with a collective rotational motion of small solvent molecules in a local area (the photoexcitation yields approximately one carrier per 15×15 nm^2 near the surface). We note

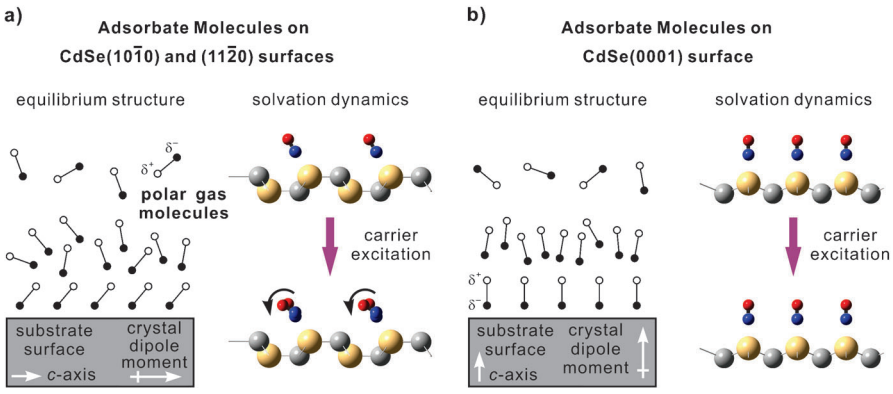

Figure 4. Solvation, reorientation, and surface dipole effects. a) Reorientation of the adsorbate molecules from their equilibrium configuration to the new structure, upon excitation of the carriers, which gives rise to a 2 ps delay. b) The prompt response of the (0001) surface (see text).

that what is monitored in Figure 3 is the secondary electrons, not the photogenerated charges. The recovery at longer times is due to carrier relaxation in CdSe, as discussed below.

The striking change in the contrast for the two surface structures is related to a dynamics change in the work function $\Delta\Phi_{dyn}$ as a result of the reorientation and movement of the adsorbate molecules. For an adsorbate-covered surface, the change in the work function at equilibrium $\Delta\Phi_{static}$ relative to an adsorbate-free surface is expressed by the Helmholtz equation [Eq. (1)].[2,28]

$$\Delta\Phi_{static} = \varepsilon_0{}^{-1}\,\sigma\mu\cos\theta \quad (1)$$

Here, ε_0 is the vacuum permittivity constant, σ the surface concentration of the adsorbed species, μ the effective molecular dipole moment, and θ is the angle between the surface normal direction and the molecular dipole (with the direction from positive to negative charge). Therefore, the observed dark contrast upon excitation can be expressed relative to the adsorbate-covered non-illuminated region [not to the adsorbate-free surface; Eq. (2)].

$$\Delta\Phi_{dyn} = \varepsilon_0{}^{-1}\,\sigma\,\Delta(\mu\cos\theta) > 0 \quad (2)$$

Given the ambient conditions used, σ is expected to have a value that represents multilayer coverage[25–28] and remain constant because of the ultrashort reorganization time involved.

With this in mind, the following microscopic picture emerges. The stable adsorbate configuration on CdSe(0001) is not significantly altered by excitation of the substrate's carriers, and this leads to no change in the ($\mu\cos\theta$) term (Figure 4b, right). A bright contrast in the difference image was, therefore, observed without a time delay, analogous to the observed behavior of CdSe in a vacuum.[29] In contrast, the carrier excitation of the $(10\bar{1}0)$ and $(11\bar{2}0)$ surfaces causes an increase in the $\Delta\Phi_{dyn}$ value because of solvation by the adsorbate layers; this increase results in a decrease in the SE generation and hence the darker contrast (less SEs). Since $\Delta\Phi_{static}$ is negative in the equilibrium state,[24,28] the rotation of the molecules is toward the horizontal direction (i.e., θ towards 90°), which is the *c*-axis direction and also the direction of the crystal dipole moment (Figure 4a, right).[30] For nonpolar molecules, the adsorbate–substrate interactions are weak, and there should be no significant effect on the work function, thus keeping the contrast behavior similar to that in a vacuum, as reported here (Figure 2d).

The effect of the solvent polarity is also apparent in the observed recovery of transients (Figure 3c). At short times, tens of ps, the recovery is similar for the different adsorbates and reflects the effect of adsorbate molecules on the direct quenching of carriers. However, at longer times the recovery gets longer and scales according to the dipole moment of the solvent used (NH_3, H_2O, and CH_3CN). This trend suggests that the polar adsorbate layer acts as a "holding potential" for the carriers, whose effect increases with polarity and which causes the lengthening of the recovery. We note that the effect of photoinduced charge transfer from the adsorbate to the surface[22–24] is not relevant in these studies, as such transfer lowers the work function and the contrast would have increased, contrary to our observations (Figure 2c, right).

Finally, we considered the possibility of the presence of a static dipole layer created across the interface between the surface atoms and the adsorbate gas molecules, which in principle could cause motion of the carriers away from the surface. We can exclude such a possibility for the following reasons. First, the dipole direction is determined by electron donation from the adsorbate (Lewis base) to the surface (Lewis acid).[31] In fact, density-functional theory calculations (see Ref. [22–24]) confirmed the partial donation of the lone pair of electrons of the adsorbates to the surface Cd atoms for both crystal surface structures, and there is no distinct difference in the binding energy. This means that a static dipole layer created in the semiconductor–adsorbate interface is of the same direction for both types of surface structures. Second, our observation of the same dynamics at positive times for the CdSe(0001) surface under polar ambient conditions and in a vacuum strongly suggests a negligible role of the static dipole layer. We note the clear delay in the onset of dynamics for CdSe$(10\bar{1}0)$ with a polar ambient environment when compared with that for CdSe-(0001) in any ambient conditions (see Figure 3B), which reflects the change in the solvent dynamics; it cannot be understood if this observation is due to the response of the photogenerated carriers to an electrostatic effect (e.g., a dipole layer or surface charging).

In conclusion, the reported development of environmental scanning ultrafast electron microscopy enables molecular solvation dynamics at materials surfaces to be imaged, thus promising femtosecond time-resolved investigation of interfacial interactions with a spatial resolution beyond the diffraction limit of visible light. Here, we have reported our first application involving the prototype CdSe surfaces with polar and nonpolar molecules, and for two different atomic surface structures. The distinct dynamic behaviors originate from the difference in interactions and structures between ambient adsorbate molecules and the surfaces involved. This approach now has the potential to explore reactivity and interfacial phenomena with the spatial and temporal scales of structural dynamics.

Experimental Section

The environmental S-UEM apparatus consists of a femtosecond fiber laser system and a modified SEM capable of environmental imaging.[16,17] The laser delivers 300 fs infrared pulses whose wavelength centers at 1030 nm and was operated at a repetition rate of 12.6 MHz for the current study. The fundamental output was frequency-doubled, directed with precision through a pyrometric window, and tightly focused onto the cooled Schottky field-emitter tip to generate photoelectron (probe) pulses. The pulses were then accelerated by a 30 kV voltage and directed by a scan coil to raster over the region of interest.

For carrier excitation of the specimen, the residual infrared beam was separated by a dichroic mirror, then frequency-doubled (515 nm, 2.41 eV) and directed and tightly focused (with a full width of about 25 μm at 1/*e* of the maximum intensity) onto the specimen in situ at an incidence angle of approximately 50° relative to the surface normal. The apparent average and peak fluences were 55 and 76 $\mu J\,cm^{-2}$, thereby yielding a carrier density of ca. $10^{19}\,cm^{-3}$ near the surface

(one carrier per ca. 15×15 nm^2). A computer-controlled optical delay line was used to define the time axis of the frames recorded. For scanning in imaging mode, a dwell time of 1 μs was used at each probed location (pixel) for stroboscopic measurements, and 64 consecutive frames were averaged to form one recorded image at a given delay time. The scanning took place over both the laser-irradiated and the unexcited regions. By delaying the arrival time of the initiating pulse at the specimen with respect to that of the electron pulse, we obtained a series of frames at well-defined times which could be made into a movie.

The specimen chamber was operated under different vacuum conditions. In a high vacuum, images were constructed after the emitted SEs were collected with a positively biased Everhart–Thornley detector. At a low vacuum, in an ambient gas of hundreds of Pascals (a density of ca. 10^{17} cm^{-3}), the emitted SEs were amplified and collected by the positively biased (ca. 450 V) gaseous SE detector located at 1 cm above the specimen. Before the arrival of the clocking light pulse, an equilibrium between the substrate and the surrounding gas molecules is established near the surface. This is the case because during the stroboscopic measurements the observations were unaltered.

CdSe single crystals were purchased from MTI Corp. The (0001) surfaces were used as acquired without additional treatments and occasionally cleaned by optical-grade methanol after several weeks. The photoinduced dynamics were not affected by the surfaces' prolonged exposure to air or by solvent cleaning. The fresh $(10\bar{1}0)$ and $(11\bar{2}0)$ surfaces were obtained by cleavage of the single crystals in air and were transferred immediately into the specimen chamber; their crystal orientations were checked by electron backscattering diffraction in our scanning electron microscope. Several $(10\bar{1}0)$ and $(11\bar{2}0)$ surfaces have been used under different vacuum conditions and in various ambient gases (also in different experimental orders) to repeat the measurements and confirm the results. These experimental observations indicate that the absorption of ambient gas molecules on fresh CdSe surfaces is not permanent and that they are not affected by the different doping level in the undoped or the Cd-doped CdSe crystals. We noticed that the cleaved surfaces began to lose their characteristic dynamics after few days in a high vacuum, which may be due to reconstruction or contamination of these surface structures after prolonged exposure.

Received: June 29, 2012
Revised: November 13, 2012
Published online: December 7, 2012

Keywords: femtochemistry · microscopy · non-equilibrium processes · solvation · surface analysis

[1] J. M. Thomas, *Design and Applications of Single-Site Heterogeneous Catalysts: Contributions to Green Chemistry, Clean Technology and Sustainability*, World Scientific Pub., Singapore, **2012**.
[2] G. A. Somorjai, Y. Li, *Introduction to surface chemistry and catalysis*, 2nd ed., Wiley, Hoboken, **2010**.
[3] P. L. Gai, E. D. Boyes, *Electron Microscopy in Heterogeneous Catalysis*, Institute of Physics Pub., Bristol, U.K., **2003**.
[4] P. L. Gai, E. D. Boyes, *Microsc. Res. Tech.* **2009**, *72*, 153.
[5] H. Yoshida, Y. Kuwauchi, J. R. Jinschek, K. J. Sun, S. Tanaka, M. Kohyama, S. Shimada, M. Haruta, S. Takeda, *Science* **2012**, *335*, 317.
[6] G. D. Danilatos, *Adv. Electron. Electron Phys.* **1988**, *71*, 109.
[7] A. M. Donald, *Nat. Mater.* **2003**, *2*, 511.
[8] J. A. McGuire, Y. R. Shen, *Science* **2006**, *313*, 1945.
[9] K. B. Eisenthal, *Chem. Rev.* **1996**, *96*, 1343.
[10] M. Bonn, C. Hess, S. Funk, J. H. Miners, B. N. J. Persson, M. Wolf, G. Ertl, *Phys. Rev. Lett.* **2000**, *84*, 4653.
[11] Z. Zhang, L. Piatkowski, H. J. Bakker, M. Bonn, *Nat. Chem.* **2011**, *3*, 888.
[12] G. Stirnemann, P. J. Rossky, J. T. Hynes, D. Laage, *Faraday Discuss.* **2010**, *146*, 263.
[13] D. E. Rosenfeld, Z. Gengeliczki, B. J. Smith, T. D. P. Stack, M. D. Fayer, *Science* **2011**, *334*, 634.
[14] A. H. Zewail, *Science* **2010**, *328*, 187.
[15] A. H. Zewail, J. M. Thomas, *4D electron microscopy: imaging in space and time*, Imperial College Press, London, **2010**.
[16] D.-S. Yang, O. F. Mohammed, A. H. Zewail, *Proc. Natl. Acad. Sci. USA* **2010**, *107*, 14993.
[17] O. F. Mohammed, D.-S. Yang, S. K. Pal, A. H. Zewail, *J. Am. Chem. Soc.* **2011**, *133*, 7708.
[18] L. Reimer, *Scanning electron microscopy: physics of image formation and microanalysis*, 2nd ed., Springer, Berlin, **1998**.
[19] B. L. Thiel, M. Toth, *J. Appl. Phys.* **2005**, *97*, 051101.
[20] S. Kirk, J. Skepper, A. M. Donald, *J. Microsc.* **2009**, *233*, 205.
[21] V. L. Colvin, M. C. Schlamp, A. P. Alivisatos, *Nature* **1994**, *370*, 354.
[22] L. Manna, L. W. Wang, R. Cingolani, A. P. Alivisatos, *J. Phys. Chem. B* **2005**, *109*, 6183.
[23] J. Y. Rempel, B. L. Trout, M. G. Bawendi, K. F. Jensen, *J. Phys. Chem. B* **2006**, *110*, 18007.
[24] I. Csik, S. P. Russo, P. Mulvaney, *J. Phys. Chem. C* **2008**, *112*, 20413.
[25] D. B. Asay, S. H. Kim, *J. Phys. Chem. B* **2005**, *109*, 16760.
[26] J. Bohr, R. A. Wogelius, P. M. Morris, S. L. S. Stipp, *Geochim. Cosmochim. Acta* **2010**, *74*, 5985.
[27] R. D. Glover, J. M. Miller, J. E. Hutchison, *ACS Nano* **2011**, *5*, 8950.
[28] K. Ozawa, K. Edamoto, *Surf. Rev. Lett.* **2002**, *9*, 717.
[29] The similar dynamics of CdSe(0001) in a vacuum and in polar ambient conditions show their independence of the surface condition and preparation. In a separate measurement, we also observed similar dynamics for the CdSe(0001) and $(10\bar{1}0)$ surfaces in a vacuum, thus excluding the different surface preparation methods as the explanation for the results reported here.
[30] As the change in work function induced by polar adsorbates is negative for both types of CdSe surfaces, the transient desorption of adsorbates would lead to an increase in the work function and therefore a dark contrast in the difference images, given the similar binding energies of the adsorbates with the two surface structures. This is in contradiction with the observation shown in Figure 2c and Figure 3. Similarly, a transient change in the adsorbate coverage (e.g., more adsorption), or any mechanism that makes no distinction for the two types of surfaces (e.g., photoemission and a fast Auger process), cannot explain the opposite behavior observed using the same polar ambient conditions.
[31] P. C. Stair, *J. Am. Chem. Soc.* **1982**, *104*, 4044.

